ChemComm

Accepted Manuscript

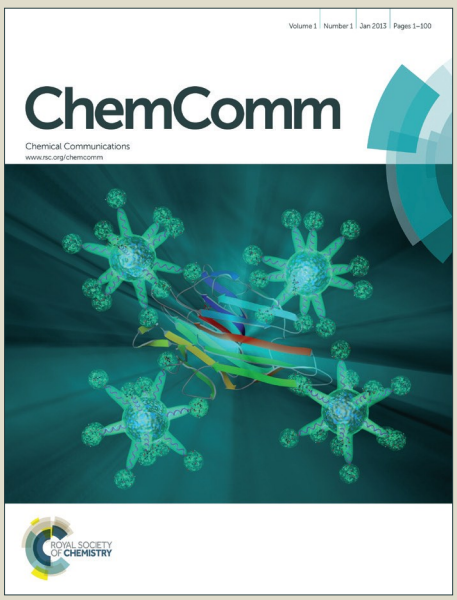

ROYAL SOCIETY OF CHEMISTRY

www.rsc.org/chemcomm

Journal Name

RSCPublishing

COMMUNICATION

Fe/N co-doped graphitic carbon bulb for high-performance oxygen reduction reaction

Cite this: DOI: 10.1039/xoxxoooooox

Ruifeng Zhou[a,b] and Shi Zhang Qiao[a*]

Received ooth January 2012,
Accepted ooth January 2012

DOI: 10.1039/xoxxoooooox

www.rsc.org/

Fe/N co-doped graphitic carbon bulb is synthesized by Prussian blue with a pyrolysis temperature as low as 550 °C. Fe facilitates formation of graphitic structure, while low temperature guarantees high level of nitrogen. The product shows excellent oxygen reduction reaction catalytic activity in both alkaline and acid electrolytes.

To reduce catalysts cost in the aqueous fuel cells is the key to their commercialization. Pt based catalysts have the best activity in the most critical reactions such oxygen reduction reaction (ORR), but their costs are too high. Therefore, a lot of efforts have been exerted to develop the alternative and inexpensive catalysts.[1] Among them, the N doped carbons[2] and their non-precious metal composites[3] are the most popular catalysts owing to their abundant source and decent performance. The metal-nitrogen-carbon systems show better performance than N doped carbons due to the metal-nitrogen synergistic effect. For example, the Fe-N doped carbon systems have shown excellent ORR performance in both alkaline and acid electrolytes.[4]

The N doped carbons are usually synthesized by pyrolyzing the carbon and nitrogen containing precursors together. The selections of proper precursors and ideal pyrolysis temperature are still challenging to obtain carbon-based catalysts with high nitrogen content, large surface area and highly graphitic structure with exceptionally high performance. Since N doped carbons naturally have worse activity per electrochemical active area than Pt,[5] they are usually made into porous structure with very high surface area and defect density to increase the active sites.[6] However, the structural defects destroy the conductivity of carbon, which is essential to electrocatalysis. On the other hand, the complicated synthesis of porous carbons also pushes up the cost of the final products. Thus, some studies focus on N doped carbons with graphitic structure, e.g. graphene and carbon nanotube, which have higher conductivity and superior catalytic performance comparing with the amorphous N doped carbons.[2] To reach acceptable graphitization, very high temperature is usually inevitable for carbon pyrolysis. Though the pyrolysis of carbon is almost completed at 500 °C, the resultant carbons don't have acceptable graphitization and conductivity until 900 °C.[4a, 7] Besides graphitization, high temperature is theoretically necessary to form proper Fe-N structure for the optimized ORR dynamics.[8] Fe-N-C material synthesized at low temperature does not show very good performance.[9] However, the high temperature synthesis also has severe drawbacks. For example, high temperature results in the loss of doped nitrogen and low surface area/active sites which are essential to ORR. The higher the synthesis temperature is, the lower the nitrogen content and surface area in the final product are. High temperature synthesis is also another origin of high cost of the final product. Thus the preparation of N-doped carbons and their non-precious metal composites (such as Fe/N co-doped carbon) with high nitrogen content, large surface area and excellent graphitization structure (high conductivity) at low temperature is extremely desirable for electroctalysis studies. However, it is rarely reported until now. To achieve above aims, the selection of precursor may be critical.

In this paper, Fe/N co-doped graphitic carbon bulb (Fe/N-gCB) is synthesized by using cheap and self-made Prussian blue (PB, formula: $Fe_4[Fe(CN)_6]_3$) as the only precursor. The pyrolysis temperature of PB can be as low as 550 °C. The Fe/N-gCB is produced by etching the iron core of core-shell pyrolyzed PB (PPB). The electron microscopy and spectroscopies show that the Fe/N-gCB is highly graphitized and retains high level of N and Fe. N_2 sorption analysis reveals that new material has a high specific surface area. The Fe/N-gCB shows excellent ORR performance, comparable to that of Pt/C in alkaline electrolyte. In acid electrolyte, Fe/N-gCB also shows fairly good ORR performance, which by far outperforms the metal-free catalysts. We proved that commonly used high temperature is not necessary for synthesis of good ORR catalyst, if proper precursors are used. Higher temperature even reduces the activity of the catalyst because of loss of nitrogen.

The details of synthesis of Fe/N-gCB and all reference materials are provided in the supporting information. The characterization of the reference materials can be found in our previous papers.[10] The transmission electron microscopy (TEM) image of the self-made PB precursor is shown in Fig S1. X-ray diffraction (XRD) pattern (Fig

S2) of the PB shows that it is partially crystallized and the mean domain size is 8 nm (from Scherrer equation). Pyrolysis of PB is monitored by thermogravimetric analysis (TGA) and the result is shown in Fig S3. The last rapid pyrolysis step of PB starts at about 500 °C. At higher than 600 °C, the PPB continuously loses weight slowly. Some more PPBs are synthesized at 600 °C, 700 °C, 800 °C and 900 °C, which are denoted as PPB-600, PPB-700, PPB-800 and PPB-900, respectively. The catalyst yield after acid leach drops dramatically as synthesis temperature increases. Nothing is left after acid leach of PPB-900. Obviously, the high temperature leads to loss of carbon. The carbon can be oxidized by trace oxygen in the atmosphere, or react with iron to form Fe_3C. Both reactions are thermodynamically favourable at any temperature, but are accelerated at higher temperature. Fig S4 shows the XRD of PPB-900, which contains both Fe and a lot of Fe_3C. Thus, 550 °C is an optimized temperature for both complete pyrolysis and high yield, which also keeps energy consumption and equipment requirement the lowest.

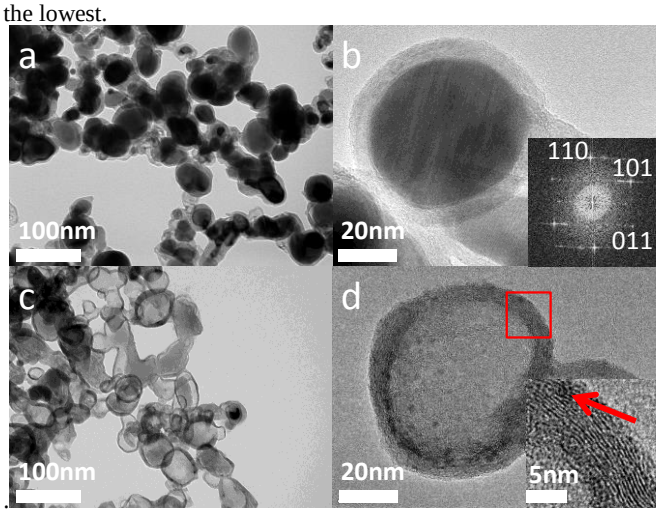

Figure 1. (a) and (b) TEM images of PPB. Inset: Fourier transformation of core. (c) and (d) TEM images of Fe/N-gCB. Inset: enlarged part in red frame. The arrow points at an iron dot.

The TEM images of the PPB are shown in Fig 1a and 1b, which exhibit spherical core-shell shape with outer diameter from 50 to 100 nm (70 nm on average of 50 particles) and shell thickness from 4 to 12 nm (6 nm on average of 50 particles). The morphology of PPB is very similar to those made from large and crystallized PB cubic.[11] This proves that the formation of core-shell structured PPB is attributed to the migration and rearrangement of atoms during pyrolysis, but not related to the morphology of the PB precursor. The Fourier transformation of the some cores (inset of Fig 1b) shows regular hexagonal pattern with spatial frequency of 5 nm^{-1}, which is in accordance with the (110) index of metallic Fe. After washing with HCl, the Fe core is etched (Fig 1c). High resolution TEM image (Fig 1d) shows that the shell has several layers with each single-layer thickness being 0.34 nm, which is typical to graphitic carbon. The growth of graphitic carbon with Fe as a catalyst has been widely reported for carbon nanotube growth,[12] in which the growth temperature can be as low as 500 to 600 °C.[13] This is in accordance with our result. When PB is used as precursor, the C source is very limited so that growth of graphene layers ceases after shell formation. The TEM analysis also shows that there are some dark dots after HCl etching, which are the Fe particles embedded in carbon shell and unexposed to HCl.

XRD patterns of the PPB and Fe/N-gCB are shown in Fig 2a. Both patterns have significant (110) and (200) peaks from metallic Fe, which are contributed by the remaining Fe particles. The XRD pattern of Fe/N-gCB also shows a peak at 26°, which is attributed to (002) plane of graphitic carbon structure, in accordance with the TEM result. This peak is not observed in PPB due to very high level of background. According to extensive TEM observation, it is found that some of the cores are amorphous (Fig S5), which contributes to the background.

There are a few key findings from X-ray photoelectron spectroscopy (XPS) survey of Fe/N-gCB and high-resolution XPS of N1s (Fig 2b). First, the nitrogen content in Fe/N-gCB is surprisingly high (> 10 %). As far as we know, the nitrogen content in pyrolyzed carbon or doped graphene is usually lower than 7 %. The high nitrogen content must thank to the very high N content in PB precursor and very low temperature of pyrolysis. The XPS of acid leached PPB-600, PPB-700 and PPB-800 are also measured (Fig S6, S7 and S8). The N content drops from 6.9 % of PPB-600 to 1 % of PPB-700. No N is detectable on PPB-800. This proves that low temperature is the key to retain high N content. Second, Fe can be identified from the survey. The calculated atom percentage of Fe from XPS curve fitting is below 1 %, but the actual Fe content is 15 % (weight ratio, about 4 % atom ratio) determined by TGA (Fig S9). The Fe signal is so weak in XPS because it is embedded in carbon layers which screen the XPS signal. Third, the pyridinic N is especially high, comparing to N-doped reduced graphene oxide (N-rGO) and amorphous N-doped mesoporous carbon nanosphere (N-MCN). A few theoretical and experimental studies have shown that the pyridinic N[14] and Fe in porphyrin structure[8b, 15] have especially high ORR activity.

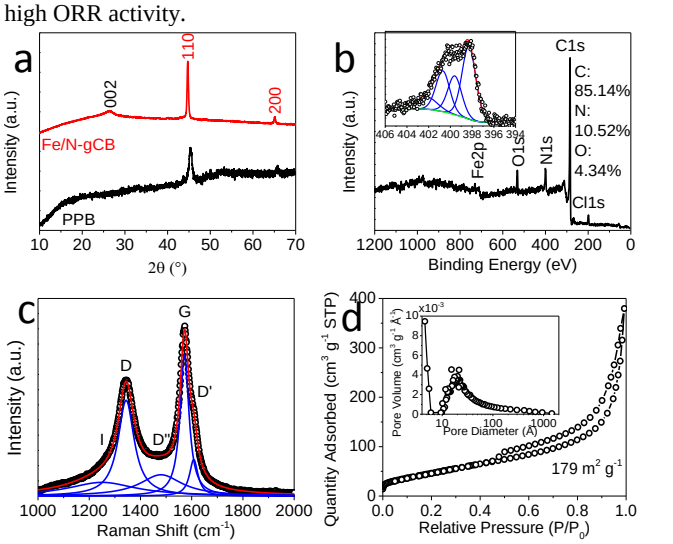

Figure 2. (a) XRD of PPB and Fe/N-gCB. The black index is assigned to graphitic carbon and red indexes are assigned to metallic Fe. (b) XPS survey of Fe/N-gCB. Inset: high resolution XPS of N1s of Fe/N-gCB. (c) Raman spectrum Fe/N-gCB. (d) N_2 isothermal sorption of Fe/N-gCB. Inset: corresponding pore distribution.

Raman spectrum of Fe/N-gCB is shown in Fig 2c while Raman spectra of N-MCN and N-rGO are shown in Fig S10 and S11 for comparison. For each Raman spectrum, the pattern can be deconvoluted with 5 bands, which are attributed to impurity (I), in-plane defect (D and D'), interstitial defects (D'') and graphitic structure (G).[16] The degree of graphitization can be estimated from the ratio of G and D bands, and the width of peaks. Obviously, the Fe/N-gCB has higher degree of graphitization than N-rGO, which inherits the graphitic structure from its precursor but suffers from defects caused by oxidation during its synthesis. As for the N-MCN, although it is carbonized at 900 °C, it still shows very wide peaks and very low G/D ratio, which prove it to be amorphous. All these spectroscopic results reveal that Fe is critical to the graphitization. In PB, the Fe content is so high and homogeneously distributed that ideal graphitic structure can form at the low temperature (550 °C). In

addition, the Fe/N-gCB has the strongest I band, which can be attributed to very high N doping.

The N_2 sorption isotherm of Fe/N-gCB is shown in Fig 2d. The material shows a specific surface area (SSA) of 179 m^2 g^{-1}, which is higher than the N-rGO (142 m^2 g^{-1}).[3b] Although single-layer graphene has very high theoretical SSA (2630 m^2 g^{-1}), it may restack easily during reducing and drying process, causing decrease of SSA. In contrast, the Fe/N-gCB has spherical structure which has exposed surface and interconnected space even after piling up. Considering Fe contributes to 15 % of the weight, whose surface is negligible, the SSA of carbon is about 210 m^2 g^{-1}. The SSA value of Fe/N-gCB corresponds to 12.5 graphitic layers (4.25 nm), which is lower than our TEM observation. This suggests that not only the inner and outer surfaces of the bulb are accessible but the shell also has pores. These pores permit the acid to etch the Fe core in PPB and contribute to high SSA. The mesopores centred at 2 nm can be attributed to the interval between bulbs when they pile up.

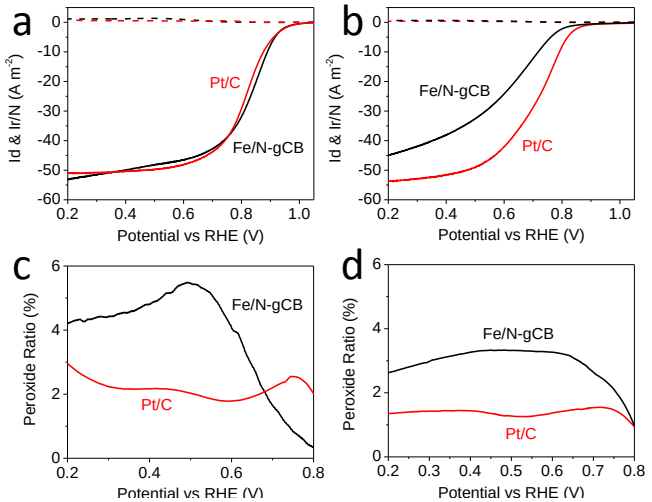

Figure 3. Normalized disk (I_d) and ring (I_r) current at 1600 rpm in alkaline (a) and acid (b) electrolyte. Both currents are normalized by the area of disk. Corresponding peroxide ratio in alkaline (c) and acid (d) electrolyte. The potential is versus reversible hydrogen electrode (RHE).

To exam the ORR performance of Fe/N-gCB, the linear scanning voltammetry (LSV) measured on rotation ring-disk electrode (RRDE) is shown in Fig 3. Commercial Pt/C is also used as a catalyst for comparison. In alkaline electrolyte (Fig 3a), the ORR onset potential of Fe/N-gCB is slightly higher than that of Pt/C and their limiting currents are almost the same (limited by mass transfer). The peroxide production of Fe/N-gCB is extremely low (< 6 %), which is only slightly higher than that of Pt/C (Fig 3c). The metal-free N doped carbons usually produce much more peroxide (up to 20 %), so the ORR on Fe/N-gCB is quite different from N doped carbons due to existence of Fe-N interaction.[3b, 10b] In acid electrolyte (Fig 3b), which is used in the mature fuel cell system, the performance of Fe/N-gCB is to some extent lower than that of Pt but not too far behind it. The peroxide ratio of Fe/N-gCB is also very low in acid electrolyte (<4 %, Fig 3d). Low peroxide production means the catalyst has high ability in peroxide activation, which can also be used in other applications such as peroxide detection in environmental sensors and peroxide reduction in peroxide based fuel cells. According to Gasteiger's benchmark, the volumic current of a non-Pt catalyst should be at least 1/10 of the Pt/C for economic viability in fuel cell applications.[17] The Fe/N-gCB catalyst obviously meets the requirement in alkaline electrolyte. In acid electrolyte, the current density of Fe/N-gCB at 0.8 V is about 1/4 of Pt/C. Assuming the density of Fe/N-gCB is 1/2 of the Pt/C, the volumic current density of Fe/N-gCB is 1/8 of Pt/C, which is also above the benchmark. As potential decreases, the volumic current ratio between Fe/N-gCb and Pt/C increases further. Considering the very low price of Fe/N-gCB, it is very competitive in practice.[4b]

We compared the ORR performance of Fe/N-gCB with electrochemically reduced graphene oxide (e-rGO), and two typical N doped carbons, N-MCN and N-rGO (Fig 4a), whose performance have been reported before.[10] N-MCN and N-rGO have much better performance than e-rGO due to nitrogen doping. However, they are much poorer than the Fe/N-gCB due to lack of Fe. N-rGO's current density is slightly higher than N-MCN, possibly due to its graphitic nature which facilitates electron transferring. Some studies speculate that the Fe core in Fe@C structure contributes to ORR catalysis in alkaline electrolyte.[11] To verify this, the electrochemical properties of Fe/N-gCB and PPB are compared. In the cyclic voltammetry (CV, Fig S12), the PPB exhibits a significant redox pair, which is attributed to transition between $Fe(OH)_2$ and $Fe(OH)_3$. This proves that the Fe core is oxidized into $Fe(OH)_x$ during ORR process. CV of Fe/N-gCB also shows the redox pair but with much lower area, because most Fe is removed by acid etching. Their LSV are shown in Fig S13. It is obvious that the PPB has slightly lower performance than Fe/N-gCB with the onset potential being about 35 mV lower. This proves that the $Fe(OH)_x$ core is not active as a ORR catalyst. Since Fe core is very heavy compared to carbon shell, the PPB at same catalyst loading will have much less active sites than the Fe/N-gCB. To verify the function of Fe, another sample named Fe/N-gCB-2 is prepared by etching PPB with more concentrated HCl (1 M), which has higher chance to remove coordinated Fe. The ORR performance of Fe/N-gCB-2 is also slightly lower than that of Fe/N-gCB (Fig S13). This proves that coordinated Fe is very important for the high activity of ORR.[8] In another sample, $Fe(OH)_x$ is combined with N-rGO at room temperature. No performance enhancement is observed. It proves again that $Fe(OH)_x$ is not active for ORR and the Fe-N bonding can be formed at elevated temperature (550 °C is enough according to our result).[8a, 18]. It is worth noting that when N-rGO is combined to Cu, Mn, Co or Ag by the same method, there is a significant ORR enhancement due to metal-nitrogen bonding.[3, 10b] In acidic electrolyte (Figure 4b), only Fe/N-gCB shows noteworthy performance. The undoped e-rGO shows the poorest performance again as expected. The N-rGO and N-MCN have very close performance, whose onset potential is about 400 mV lower than that of the Fe/N-gCB. That means they are almost useless in fuel cells. Obviously, N doping has improved the ORR performance a lot in acid electrolyte, but the Fe-N interaction is more crucial to make it competitive to Pt/C in practice. The ORR performance of acid leached PBB-600, PBB-700 and PBB-800 are also tested for comparison (Fig S14 and S15). In alkaline electrolyte, the performance decreases slightly on PPB-600 and PPB-700, but drops dramatically on PPB-800. The trend is in accordance with the trend of N content. The performance change is more significant in acid electrolyte. A possible reason is that in acid electrolyte, the ORR performance is more sensitive to local atomic structure which has changed from 550 °C to 600 °C.

The Tafel plots of these typical catalysts are also provided to give some hints of ORR mechanism. In alkaline electrolyte, the N-MCN and N-rGO show exactly the same Tafel slope (Fig 4c). This implies that they share the same ORR mechanism at low overpotential. The Fe/N-gCN and Pt/C also have very close Tafel slopes so they have the same ORR mechanism, although they are completely different materials. The coordinate Fe atoms are supposed to create new active sites (Fe atom itself in addition C bonded to N) with a very high catalytic activity whose mechanism is similar to Pt. This is in accordance with theoretical calculations.[8b, 15] The reaction rate on Fe active site is much higher than that on the carbon site, so that a Tafel slope different from that of N doped carbon is observed. The Fe/N-

gCB-2, which has lower Fe content, shows exactly the same Tafel slope as the Fe/N-gCB but lower exchange current density (Fig S16). The Tafel plot of PPB is also the same. Both of PPB and Fe/N-gCB-2 have same Fe-N-C structure as Fe/N-gCB but less active site density. This proves again that the Fe atoms are the main active centres in Fe-N-C structure. In acid electrolyte, Pt/C keeps the same Tafel slope as in alkaline electrolyte, showing an identical mechanism (Fig 4c, d). The Tafel slope of Fe/N-gCB in acid electrolyte shows a little higher than that in alkaline electrolyte (Fig 4c, d). A possible reason is that the acid changes part of local atomic structure the Fe-N active centres.

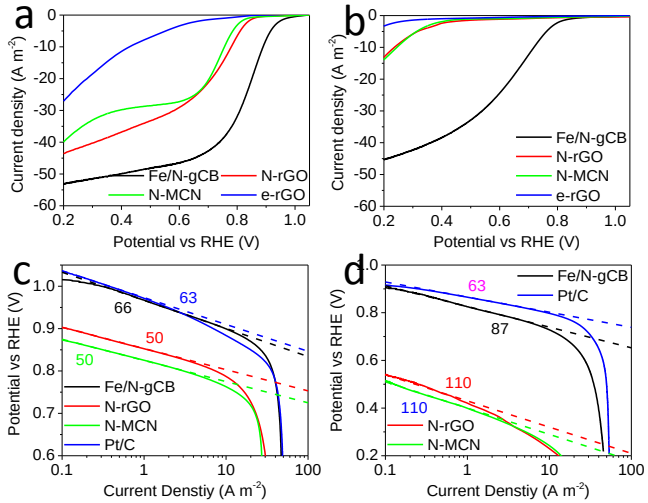

Figure 4. Normalized disk current at 1600 rpm in alkaline (a) and acid (b) electrolyte. Corresponding Tafel plot in alkaline (c) and acid (d) electrolyte. The numbers are Tafel slopes in mV per decade.

Finally we checked the ORR stability of Fe/N-gCB. The current retention vs time lapse plot is shown in Fig S17. In alkaline electrolyte, the Fe/N-gCB shows very good stability in 50,000 s test, remaining 90 % of the initial current. In acidic electrolyte, the stability is to some extent lower (70 %). It is reasonable because Fe can be etched by strong acid like H_2SO_4 used in this experiment, especially with saturated O_2. Although the Fe/N-gCB is washed with HCl before testing to remove most metallic Fe, the remaining coordinated Fe can still be etched by long-term reaction. This, on the other hand, proves the importance of Fe in Fe/N-gCB for ORR. The LSVs of the Fe/N-gCB before and after 50,000 s test are shown in Fig S18 and S19. Current densities are slightly lower in both acid and alkaline electrolyte after 50,000 s test than the original ones.

Conclusions

In conclusion, we have synthesized novel Fe/N-gCB as a high-performance ORR catalyst. The key findings include: 1) Highly graphitic and lowly defective carbon with extraordinarily high N content can be synthesized at low temperature of 550 °C. 2) High Fe content facilitates the formation of high specific surface area and graphitic structure at low temperature. 3) The low temperature process retains high level of N. Both yield and N content decrease as synthesis temperature increases. 4) Fe/N-gCB shows comparable performance with Pt/C in alkaline electrolyte and adequate performance in acidic electrolyte. 5) Only the Fe coordinated to N in the shell can contribute ORR activity. 6) High temperature synthesis reduces the activity of final product. We believe the Fe/N-gCB is a very promising catalyst for ORR and our findings are informative for future study on ORR catalysts.

Acknowledgements

This work is financially supported by the Australian Research Council (ARC) through the Discovery Project programs (DP130104459 and DP140104062).

Notes and references

[a] School of Chemical Engineering, University of Adelaide, Adelaide SA 5005 Australia. Email: s.qiao@adelaide.edu.au

[b] Australian Institute for Bioengineering and Nanotechnology, University of Queensland, St Lucia QLD 4072 Australia.

Electronic Supplementary Information (ESI) available: Synthesis of material, supporting figures. See DOI: 10.1039/c000000x/

1(a) Y. Zheng, Y. Jiao, M. Jaroniec, Y. Jin and S. Z. Qiao, *Small*, 2012, **8**, 3550; (b) Y. Zheng, J. Liu, J. Liang, M. Jaroniec and S. Z. Qiao, *Energy Environ. Sci.*, 2012, **5**, 6717.

2(a) L. T. Qu, Y. Liu, J. B. Baek and L. M. Dai, *ACS Nano*, 2010, **4**, 1321; (b) K. P. Gong, F. Du, Z. H. Xia, M. Durstock and L. M. Dai, *Science*, 2009, **323**, 760.

3(a) Y. Liang, Y. Li, H. Wang, J. Zhou, J. Wang, T. Regier and H. Dai, *Nat. Mater.*, 2011, **10**, 780; (b) R. F. Zhou, Y. Zheng, D. Hulicova-Jurcakova and S. Z. Qiao, *J. Mater. Chem. A*, 2013, **1**, 13179; (c) J. Duan, Y. Zheng, S. Chen, Y. Tang, M. Jaroniec and S. Qiao, *Chem. Commun.*, 2013, **49**, 7705.

4(a) J. Liang, R. F. Zhou, X. M. Chen, Y. H. Tang and S. Z. Qiao, *Adv. Mater.*, 2014, **26**, 6074; (b) Y. G. Li, W. Zhou, H. L. Wang, L. M. Xie, Y. Y. Liang, F. Wei, J. C. Idrobo, S. J. Pennycook and H. J. Dai, *Nat. Nanotech.*, 2012, **7**, 394; (c) M. Lefevre, E. Proietti, F. Jaouen and J. P. Dodelet, *Science*, 2009, **324**, 71.

5 Y. Jiao, Y. Zheng, M. Jaroniec and S. Z. Qiao, *J. Am. Chem. Soc.*, 2014, **136**, 4394.

6(a) Y. J. Zhang, M. Chu, L. Yang, W. F. Deng, Y. M. Tan, M. Ma and Q. J. Xie, *Chem. Commun.*, 2014, **50**, 6382; (b) W. Wei, H. Liang, K. Parvez, X. Zhuang, X. Feng and K. Muellen, *Angew. Chem. Int. Ed.*, 2014, **53**, 1570.

7(a) D. Geng, Y. Chen, Y. Chen, Y. Li, R. Li, X. Sun, S. Ye and S. Knights, *Energy Environ. Sci.*, 2011, **4**, 760; (b) R. L. Liu, D. Q. Wu, X. L. Feng and K. Mullen, *Angew. Chem. Int. Ed.*, 2010, **49**, 2565.

8(a) N. Ramaswamy, U. Tylus, Q. Y. Jia and S. Mukerjee, *J. Am. Chem. Soc.*, 2013, **135**, 15443; (b) S. Kattel and G. F. Wang, *J. Mater. Chem. A*, 2013, **1**, 10790.

9 Z. S. Wu, S. B. Yang, Y. Sun, K. Parvez, X. L. Feng and K. Mullen, *J. Am. Chem. Soc.*, 2012, **134**, 9082.

10(a) T. Yang, J. Liu, R. Zhou, Z. Chen, H. Xu, S. Z. Qiao and M. J. Monteiro, *J. Mater. Chem. A*, 2014, **2**, 18139; (b) R. F. Zhou and S. Z. Qiao, *Chem. Mater.*, 2014, **26**, 5868.

11 Y. Hou, T. Huang, Z. Wen, S. Mao, S. Cui and J. Chen, *Adv. Energy Mater.*, 2014, **4**.

12 X. Feng, K. Liu, X. Xie, R. Zhou, L. Zhang, Q. Li, S. Fan and K. Jiang, *J. Phys. Chem. C*, 2009, **113**, 9623.

13(a) Y. M. Shyu and F. C. N. Hong, *Mater. Chem. Phys.*, 2001, **72**, 223; (b) Y. J. Li, Z. Sun, S. P. Lau, G. Y. Chen and B. K. Tay, *Appl. Phys. Lett.*, 2001, **79**, 1670.

14(a) L. Zhang and Z. Xia, *J. Phys. Chem. C*, 2011, **115**, 11170; (b) J. Chen, X. Wang, X. Cui, G. Yang and W. Zheng, *Chem. Commun.*, 2014, **50**, 557.

15 C. E. Szakacs, M. Lefevre, U. I. Kramm, J. P. Dodelet and F. Vidal, *Phys. Chem. Chem. Phys.*, 2014, **16**, 13654.

16 A. Cuesta, P. Dhamelincourt, J. Laureyns, A. Martinezalonso and J. M. D. Tascon, *Carbon*, 1994, **32**, 1523.

17 H. A. Gasteiger, S. S. Kocha, B. Sompalli and F. T. Wagner, *Appl. Catal., B*, 2005, **56**, 9.

18 U. I. Kramm, M. Lefevre, N. Larouche, D. Schmeisser and J. P. Dodelet, *J. Am. Chem. Soc.*, 2014, **136**, 978.

